JOURNAL OF Materials CHEMISTRY

Time-resolved *in situ* X-ray diffraction study of the liquid-phase reconstruction of Mg–Al–carbonate hydrotalcite-like compounds

Franck Millange, Richard I. Walton and Dermot O'Hare*

Inorganic Chemistry Laboratory, South Parks Road, Oxford, UK OX1 3QR.
E-mail: dermot.ohare@chem.ox.ac.uk

Received 28th January 2000, Accepted 5th April 2000
Published on the Web 24th May 2000

The brucite-like Mg^{2+}/Al^{3+} layered double hydroxide (LDH) was synthesized by using the coprecipitation method and calcined at a variety of temperatures. The starting LDH and the calcination products (mixtures of binary oxides and spinels) were characterized by X-ray diffraction, IR spectroscopies and thermogravimetric analysis. These techniques allowed us to confirm that the double hydroxide possesses a brucite-like structure in which cations are octahedrally arranged. At moderate temperatures, the calcination products have a MgO-like structure where Al ions are dissolved in the lattice to form a solid solution. Calcination at high temperatures (up to 1000 °C) yields a mixture of well-crystallized phases corresponding to MgO and $MgAl_2O_4$ (spinel). The reconstruction of layered double hydroxides from material calcined at 400 °C has been studied *in situ* by time resolved energy dispersive X-ray diffraction (EDXRD). Kinetic data for the reaction have been determined and modelled using the Avrami–Erofe'ev nucleation–growth model, consistent with the process taking place by dissolution of the starting material and crystallisation of the LDH from the solution.

Introduction

Layered materials that are able to intercalate neutral guest molecules or to exchange interlayer inorganic or organic anions receive considerable attention. Although a variety of layered materials possessing cation-exchange properties are known (such as cationic clays or metal phosphates and phosphonates), layered materials that possess anion-exchange properties are comparatively rare.[1] Layered double hydroxides (LDHs) and synthetic anionic clays having hydrotalcite (HT)-like structures have received interest in recent years due to their potential applications in various technologies as anion exchangers, adsorbents, ionic conductors, catalysts, and catalyst supports.[2–6] The structure of LDHs was first elucidated by Allmann for the MgFe-LDH (pyroaurite and sjogrenite)[7] and by Brown and Gastuche for the MgAl-LDH (hydrotalcite and manasseite).[8] Layered double hydroxides can be structurally described as containing brucite ($Mg(OH)_2$)-like layers in which some divalent metal cations have been substituted by trivalent ions to form positively charged sheets. The metal cations occupy the centers of octahedra whose vertices are hydroxide ions. These octahedra are connected to each other by edge sharing to form an infinite sheet. The cationic charge created in the layers is compensated by the presence of hydrated anions between the stacked sheets.

LDHs can be represented by the general formula: $[M^{II}_{1-x}M^{III}_x(OH)_2](A^{n-}_{x/n})\cdot zH_2O$, where M^{II} and M^{III} are di- and trivalent metal cations, respectively, that occupy octahedral positions in hydroxide layers. The value of x ($x = M^{III}/(M^{II}+M^{III})$) ranges between 0.20 and 0.33 for the MgAl-system[9] and A^{n-} is the interlayer charge-compensating anion such as CO_3^{2-}, NO_3^-, or Cl^-. These ionic layered materials have been called hydrotalcite-like compounds in reference to the structural similarity to the mineral hydrotalcite, $[Mg_3Al(OH)_8][(CO_3)_{0.5}]\cdot 2H_2O$. A large number of LDHs with a wide variety of M^{II}–M^{III} cation pairs as well as M^{I}–M^{III} cation pairs (*e.g.* Li–Al) with different anions in the interlayer and their physicochemical properties have been reported.[10–12]

Direct synthesis of LDHs can be conducted by various methods, *e.g.* coprecipitation,[13] the salt-oxide method,[14] hydrothermal synthesis,[13] as well as lesser studied methods.[15] Indirect synthesis has traditionally been conducted using three main techniques: (i) direct anion exchange, using an LDH intercalated with chloride or nitrate as the precursor; (ii) anion exchange by elimination of the precursor interlamellar species (usually carbonate or terephthalate) susceptible to acid attack; and (iii) reconstruction of the material obtained by the calcination of an LDH intercalated with carbonate (eventually others), in a solution containing the anion of interest. Monitoring structural changes during calcination has been the aim of numerous studies.[2,16–19] For the Mg–Al–carbonate hydrotalcite the layered structure is maintained up to *ca.* 360 °C. Then a poorly crystalline phase is formed, and crystallisation of MgO starts. Location of Al^{III} cations has not been fully resolved, and formation of amorphous Al oxides, or a solid solution in the MgO structure, have both been claimed. This material has been called a layered double oxide (LDO) and on rehydration the LDH is produced with the incorporation of other anions. Calcination above 800 °C results in the formation of MgO and $MgAl_2O_4$ spinel.[20–22]

In the present paper, we report on the structural changes taking place during the thermal decomposition of the Mg–Al–carbonate hydrotalcite and during the controlled reconstruction of the layered structure followed by time resolved *in situ* energy dispersive X-ray diffraction experiments.

Experimental details

Preparation of Mg–Al-LDH

The initial HT-compounds for calcination and reconstruction were prepared using the coprecipitation method at room temperature by reacting aqueous solutions containing a mixture of $Mg(NO_3)_2\cdot 6H_2O$, $Al(NO_3)_3\cdot 6H_2O$, NaOH, and Na_2CO_3 in the ratio 3 : 1 : 1.5 : 2. The mixture was maintained at pH 10 by dropwise addition of 1 M NaOH aqueous solution with vigorous stirring during precipitation. The Mg : Al atomic ratio in the starting solution was adjusted to 1 : 3. Once addition was completed, the resulting precipitate was aged at 70 °C for 24 h under stirring in a magnetic stirrer. The precipitate was then isolated by filtration, washed thoroughly

DOI: 10.1039/b002827o

with deionized water several times and dried in an air oven at 70 °C overnight. In order to follow the destruction process of the layered structure, a 1 g sample was calcined in air for 2 h at different temperatures from 100 °C to 1000 °C.

Materials characterisation

Differential thermal analysis (DTA) and thermogravimetric analysis (TGA) were performed on a Rheometric Scientific STA 1500 from 298 K to 1273 K at 5 K min^{-1} in dry air.

The HT-Mg/Al and the resulting samples calcined at different temperatures were stored in a dessicator before FT-IR measurements. Samples were finely ground for one minute, combined with oven dried spectroscopic grade KBr having a refractive index of 1.559 and a particle size of 5–20 μm in a 15 : 85 ratio, and pressed into a disc. The spectrum of each sample was recorded in triplicate by accumulating 64 scans at 8 cm^{-1} resolution between 400–4000 cm^{-1} using a Mattson Instruments Galaxy Series 6020 FT-IR.

Powder X-ray diffraction patterns (XRD) were recorded on a Siemens D-5000 diffractometer using graphite monochromated Cu-K_α radiation and operating at 40 kV and 30 mV. For identification purposes, scans were performed at 0.02° (2θ) over the 2θ range 6–80° using 10 s per step. Measurements of *in situ* XRD were carried out in the temperature range of 30–1020 °C (step 20 °C) in wet He by using a Siemens D-5000 X-ray diffractometer equipped with a high temperature attachment (Anton Paar HTK 1200); with a sequential temperature rate of increase of 5 °C min^{-1} and with no temperature holding time before each measurement.

The time resolved *in situ* energy dispersive X-ray diffraction (EDXRD) experiments were performed on Station 16.4 of the UK Synchrotron Radiation Source (SRS) at the Daresbury Laboratory, Cheshire. The SRS is a low emission storage ring with an electron beam energy of 2 GeV. Station 16.4 receives usable X-ray flux in the range 15–120 keV with a maximum flux in the region of 3×10^{10} photons s^{-1}. Experimental apparatus has been developed over a number of years by O'Hare *et al.* to allow the course of intercalation and hydrothermal reactions to be studied under real laboratory conditions using time resolved *in situ* EDXRD.[23,24]

Results and discussion

Synthesis

$[Mg_3Al(OH)_8][(CO_3)_{0.5}]\cdot 2H_2O$ was prepared using the coprecipitation method at room temperature from an aqueous solution containing a mixture of $Mg(NO_3)_2\cdot 6H_2O$, $Al(NO_3)_3\cdot 6H_2O$, NaOH, and Na_2CO_3 at a constant pH. Elemental microanalysis of the isolated solid confirmed the Mg : Al ratio as 3 : 1. The Mg : Al ratio remains constant (within error of analysis techniques) before and after reconstruction and is not affected by the temperature of the reconstruction.

Thermal properties

The thermal stability of the LDH was examined by simultaneous TG/DTA experiments. Fig. 1 depicts the TG and DTA curves of the representative $[Mg_3Al(OH)_8][(CO_3)_{0.5}]\cdot 2H_2O$ sample. The thermal decomposition of hydrotalcite-like compounds has been widely studied.[20,22,25] The TGA curve exhibits three main regions over the temperature ranges 25–240 °C, 240–480 °C and 480–1000 °C, which involve a total weight loss of 44.9%. The TGA results indicate that the LDH is thermally stable up to 240 °C. The weight loss below this temperature (first endothermic peak observed at 220 °C) is ascribed to external surface water and to interlamellar water molecules. The second weight loss between 240 °C and 480 °C has been ascribed to the dehydroxylation of the brucite-like

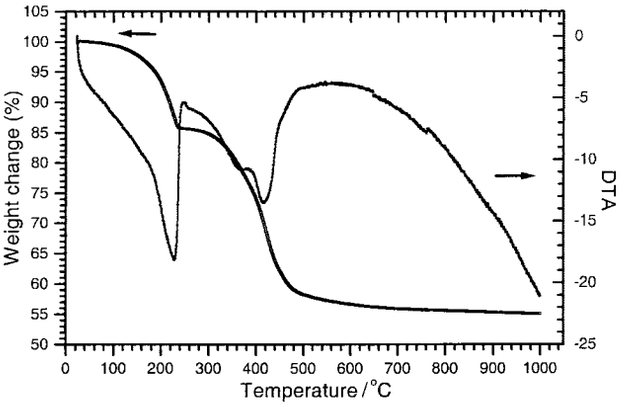

Fig. 1 DTA/TG thermal analysis of the HT-Mg–Al–CO_3.

layers along with anion decomposition (decarbonation process). Over this range of temperature, LDHs produce metal oxides as observed by HTXRD. The DTA curve shows an endothermic peak at 420 °C with a shoulder around 360 °C, thus indicating almost concomitant dehydroxylation and decarbonation processes.[9] Finally, the third weight loss, of lesser significance than the previous two, has been assigned to a progressive elimination of the volatile anions.[26]

X-Ray diffraction studies

The XRD analysis of the as prepared $[Mg_3Al(OH)_8][(CO_3)_{0.5}]\cdot 2H_2O$ (Mg–Al–CO_3-LDH) revealed a high degree of crystallinity. The XRD pattern of the LDH (Fig. 2) is similar to those previously found by Reichle *et al.* in Mg–Al-LDHs.[27] This XRD pattern exhibits some common features of layered materials (*e.g.* narrow, symmetric, strong lines at low 2θ values and weaker, less symmetric lines at high 2θ values).[28] The (00*l*) reflections (003), (006), (009) are easily recognised, although the last one shows overlap with the (102) reflection resulting in a broad signal. Furthermore, the two reflections of (110) and (113) can be clearly distinguished between 60° and 63° 2θ.

The (00*l*) reflections are characterised by high intensities combined with broad lineshapes indicating that the hydrotalcites are of relatively high crystallinity but with very small crystallites. The average crystallite sizes of the compound were calculated from the (003) and (006) reflections employing the Debye–Scherrer equation, with $L = 0.89\lambda/(\beta(\theta)\cos\theta)$, where L is the crystallite size, λ is the wavelength of the radiation used, $\beta(\theta)$ is the full width at half maximum (FWHM) and θ is the Bragg diffraction angle, giving a minimum value of $L \approx 325$ Å. A very small impurity, Al_2O_3 (corundum) has been detected in the XRD pattern (Fig. 2). The diffraction maxima correspond-

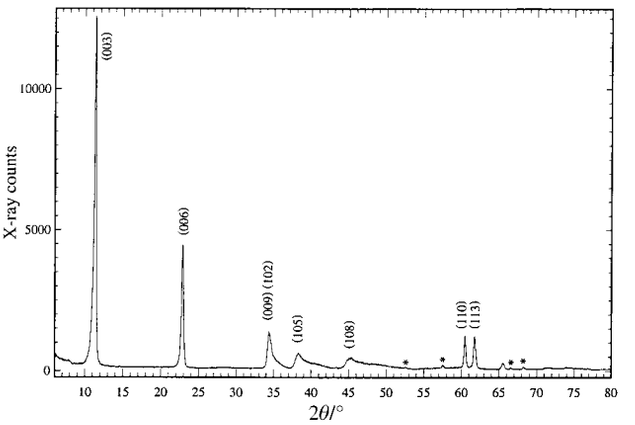

Fig. 2 X-Ray diffraction pattern of the HT-Mg–Al–CO_3 at room temperature. The asterisks indicate reflections due to the impurity Al_2O_3.

ing to diffraction by basal planes at 7.8 Å, 3.9 Å and 2.6 Å are similar to those previously reported in the literature and correspond to a well crystallised hydrotalcite-like structure. Assuming a 3R stacking of the layers[29] and from the positions of the peaks due to planes (003) and (110), the lattice parameters were calculated as $c = 23.32(2)$ Å and $a = 3.06(1)$ Å. The former corresponds to three times the layer-to-layer distance, while the latter corresponds to the average metal–metal distance within the layers. The interlayer space, assuming 4.8 Å for the width of the brucite-like layer,[30] is 3 Å, in agreement with the location of the carbonate anions with their molecular planes parallel to the brucite-like layers.

Thermal calcination of LDH often produces very reactive mixed oxides, previously called layered double oxides (LDOs). The determination of crystalline phases formed during calcination at various temperatures is useful to assess the thermal stability of the materials.[20–22,25,28] A general view in Fig. 3 shows the whole HTXRD pattern of Mg–Al–CO_3-LDH synthesized with the ratio Mg/Al = 3. There are three temperature regions which are classified by a common HTXRD pattern in each region: 20–160 °C, 180–360 °C and 380–1020 °C. Sharp and intense patterns were observed in the first two temperature regions. On calcination up to 160 °C (the first region), no appreciable change is observed in the HTXRD patterns, which are almost identical (relative intensities and positions of the peaks). The removal of any physisorbed water does not modify the layer structure. When the sample is calcined between 160 °C and 360 °C, the XRD patterns are slightly weaker and broader, and the peak corrresponding to diffraction by plane (003) shifts from 7.8 Å to 6.8 Å (Fig. 3). At a calcination temperature of 240 °C, the dehydration process (as evidenced from DTA/TG) induces a decrease in basal spacing of about 1 Å.[20,31] It is noted that the intensity of the second harmonic, reflection (006), decreases much more than that of the peak for the plane (003). At the same time, the (10*l*) reflections close to $2\theta = 60°$ become broader due to some disorder in the structure, but overall it can be concluded that the sample partially retains a layered structure with similar metal–metal distances in the layer (approximatively same *a* parameter). On increasing temperature further, the absence of diffraction peaks corresponding to the LDH phase revealed that the layer structure is completely destroyed in agreement with the dehydroxylation of the brucite-like layers along with anion decomposition (as observed from DTA/TG). For example, calcination at 380 °C results in a collapse of the layered structure and only three broad peaks are recorded, with positions which roughly coincide with those of a mixed oxide phase with an MgO-like structure (periclase). This result is consistent with previous findings that MgO is the sole crystalline phase expected to occur at these calcination temperatures. However, the lattice constant of the MgO-like structure at 380 °C is lower than that of the pure MgO (4.21 Å), indicating that Al ions are dissolved in the lattice to form a solid solution. This is consistent with a previous report of an EXAFS study that showed the poorly-ordered oxide contains aluminium in a tetrahedral environment.[32] No major changes are observed as the calcination temperature is increased up to 850 °C. The sharpness of the peaks increases with increasing calcination temperature, in line with the results of progressive increase of the crystallinity due to sintering of the material. Finally, new peaks are also detected due to the formation of the $MgAl_2O_4$ spinel-like compound upon raising the temperature up to 1020 °C. It should be mentioned that the structure of $MgAl_2O_4$ is a normal spinel wherein the Mg^{2+} and Al^{3+} occupy the tetrahedral and octahedral sites, respectively. In the range of 380 °C to 800 °C, the lattice parameter *a* for the MgO compound increases gradually, and rapidly above 800 °C. This result confirms that Al ions, which have a smaller ionic radius than Mg ions, are progressively released from the MgO-like structure to spinel $MgAl_2O_4$.[20]

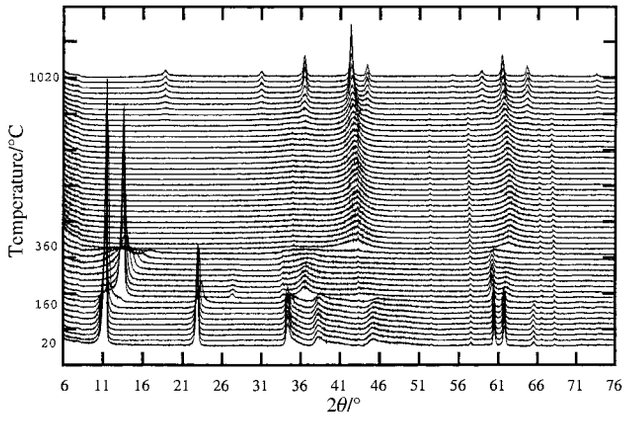

Fig. 3 *In situ* HTXRD diffraction patterns of the HT-Mg–Al–CO_3 at temperatures between 20–1020 °C (step 20 °C).

Infra-red studies

The FT-IR spectrum of Mg–Al–CO_3-LDH in the region between 500 and 4000 cm^{-1} is shown in Fig. 4. The room temperature FT-IR shows characteristic bands for Mg–Al-LDH intercalated with CO_3^{2-} as the counteranion.[22,26] Two broad and intense bands around 3550 cm^{-1} and 3100 cm^{-1} are observed, which are attributed to the twisting vibrations of physisorbed water, vibrations of the structural OH^- groups, characteristic valency vibrations of OH···OH, and/or characteristic stretching vibrations of M–OH in hydroxycarbonates. The corresponding deformation mode is recorded around 1650 cm^{-1} (δ_{HOH}). In fact, the band component analysis of the hydroxyl-stretching region between 2500 cm^{-1} and 4000 cm^{-1} performed recently by Kloprogge and Frost[33] has revealed the presence of four bands: (i) a first band observed around 3000 cm^{-1} interpreted as the CO_3^{2-}–H_2O bridging mode of carbonate and water in the interlayer, (ii) a second band assigned to hydrogen-bonded interlayer water around 3300 cm^{-1} and two bands assigned to different M–OH stretching modes (one band near 3470 cm^{-1} seems to be mainly due to the Al–OH bond with a small influence of nearby Mg cations while the other band near 3600 cm^{-1} can not be clearly assigned to either Mg– or Al–OH bonds). The intermediate frequency region between 1200 cm^{-1} and 1800 cm^{-1} is characterised by the bending mode of interlayer water around 1655 cm^{-1} as previously mentioned and the ν_3 (asymmetric stretching) around 1377 cm^{-1} associated with the interlayer carbonate. In the low frequency region (between 400 cm^{-1} and 1200 cm^{-1}), the two bands around 670 cm^{-1} and

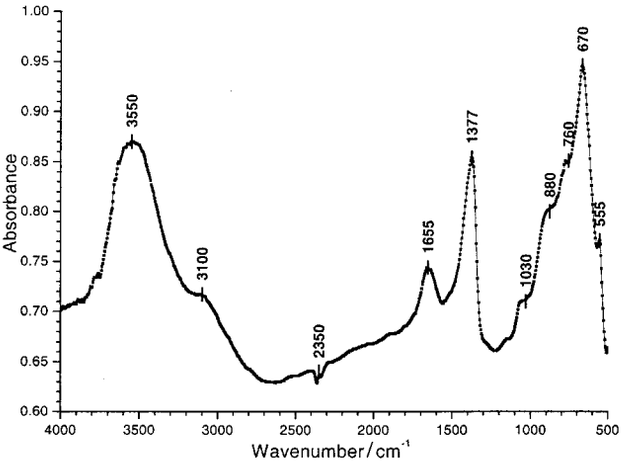

Fig. 4 Infrared absorption spectrum for the HT-Mg–Al–CO_3 recorded at room temperature.

880 cm^{-1} are characteristic for the v_4 (in-plane bending) and the v_2 (out-of-plane deformation) of CO_3^{2-} ion. The other bands below 1000 cm^{-1} are generally ascribed to the M–O skeletal vibrations. The bands around 555 cm^{-1} and 760 cm^{-1} can be assigned to the translation modes of the hydroxyl groups mainly influenced by the trivalent aluminium with the corresponding deformation modes around 925 cm^{-1} and 1050 cm^{-1} while the bands assigned to the translation modes of the hydroxyl groups mainly influenced by the divalent magnesium are expected around 635 cm^{-1}, 600 cm^{-1} and 590 cm^{-1}.[25]

When the HT was heated up to 400 °C, the v_3 band of carbonates splits into two bands at 1377 cm^{-1} and 1520 cm^{-1} (Fig. 5). These two bands are in excellent agreement with those found for bridged bidentate CO_3 complexes. The carbonate exists as bridged bidentate ligands, between 180 °C and 360 °C, at which interlayer water is lost. Above 400 °C, the FT-IR spectra are markedly different from the previous ones. The spectra show prominent bands at 450 cm^{-1} corresponding to characteristic vibrations of the oxides (MgO, Al_2O_3). The spectra also include a broad band at 1450 cm^{-1} typical of O–C–O vibrations for adsorbed (non-interlayer) carbonate on the surface of the mixed oxides formed upon calcination, together with carbonate and water reversibly adsorbed on the oxide surfaces.[34] The frequency of this band (1450 cm^{-1}) occurs at slightly higher frequency than that for interlayer carbonate (1377 cm^{-1}), which confirms that the remaining carbonates coordinate weakly with cations. At higher temperature (1000 °C), several new bands are observed in the region 450–550 cm^{-1} which correspond to vibration bands of MgO and spinel phases.[25,28]

Time resolved *in situ* X-ray diffraction study of the LDH reconstruction

Energy-dispersive X-ray diffraction (EDXRD), using white-beam synchrotron-generated X-rays, permits the use of large sample cells because the high intensity of the incident radiation is sufficient to penetrate thick-walled vessels. Since diffraction data are measured by a fixed detector only small windows are required for the passage of X-rays, and reaction cells can be constructed to resemble laboratory apparatus in size and construction.[23,24,35] Although the energy-discriminating detector is of inherently low resolution ($\Delta E/E$ *ca.* 0.01), the short data acquisition time (typically less than one minute) allows the evolution or decay of Bragg reflections to be monitored in real time and thus kinetic data can be extracted for chemical processes under real reaction conditions. In the current work, the reconstruction of the poorly crystalline LDO prepared by calcination of the Mg–Al-LDH at 400 °C using 0.8 M sodium carbonate solution was followed at a number of temperatures. In each experiment, 1.38 g of the LDO was placed with 10 cm^3 of distilled water in a 30 cm^3 Pyrex ampoule, shaken with 8 g of the sodium carbonate solution (a 1.5 molar excess of CO_3^{2-}) and transferred to a pre-heated aluminium heating block which contains windows for the X-ray beam to pass through.[23] The reaction was stirred by means of a magnetic stirring device so that a homogenous portion of the sample remained in the beam at all times. Energy-dispersive diffraction patterns were recorded every 30 s by a detector situated at 2.51°. Fig. 6 shows part of the EDXRD patterns at selected times during the course of a typical reconstruction, and shows that the appearance of the crystalline LDH can be followed by monitoring the intensity of the strong (003) Bragg reflection at ≈36.4 keV (7.8 Å). The area and peak-width (FWHM) of this diffraction feature were determined using an automated Gaussian-fitting routine[36] and results are shown in Fig. 7 and 8 for three of the temperatures studied.

The first simple kinetic information that the *in situ* EDXRD experiment has provided is the time-scale of the reaction. The reconstruction process occurs rapidly, as evidenced by the almost immediate appearance of the LDH (003) Bragg reflection at all temperatures studied, and this diffraction feature then reaches its maximum intensity after only ≈1 hour for the elevated temperatures used. At room temperature the

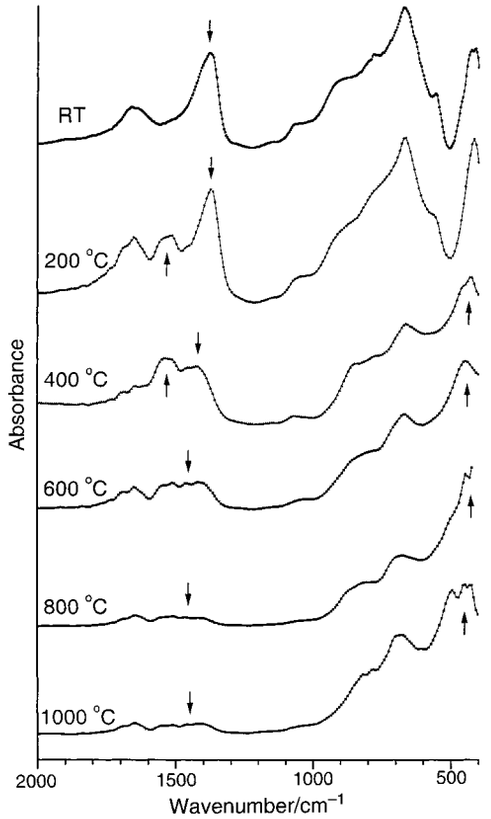

Fig. 5 Infrared absorption spectra for the HT-Mg–Al–CO_3 heated at various temperatures in air for 2 h. Several bands are marked.

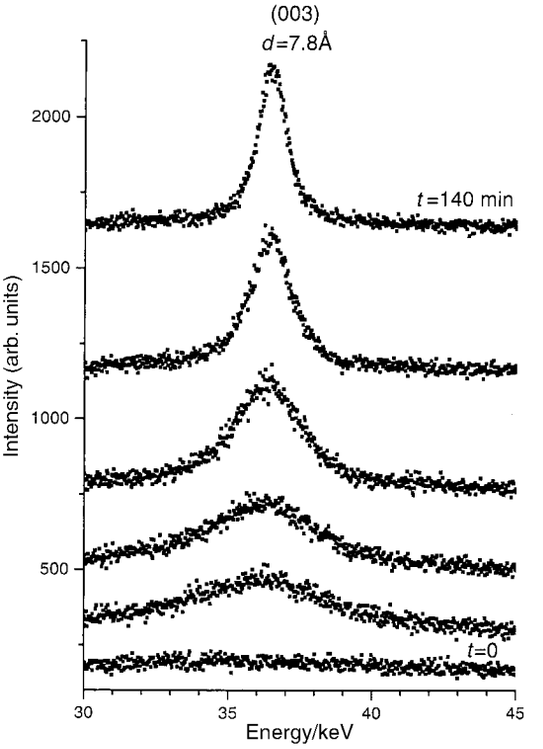

Fig. 6 Part of the EDXRD spectra measured during the crystallisation of Mg–Al-LDH from amorphous LDO and sodium carbonate solution at 60 °C at selected times. Each spectrum was acquired in 30 s.

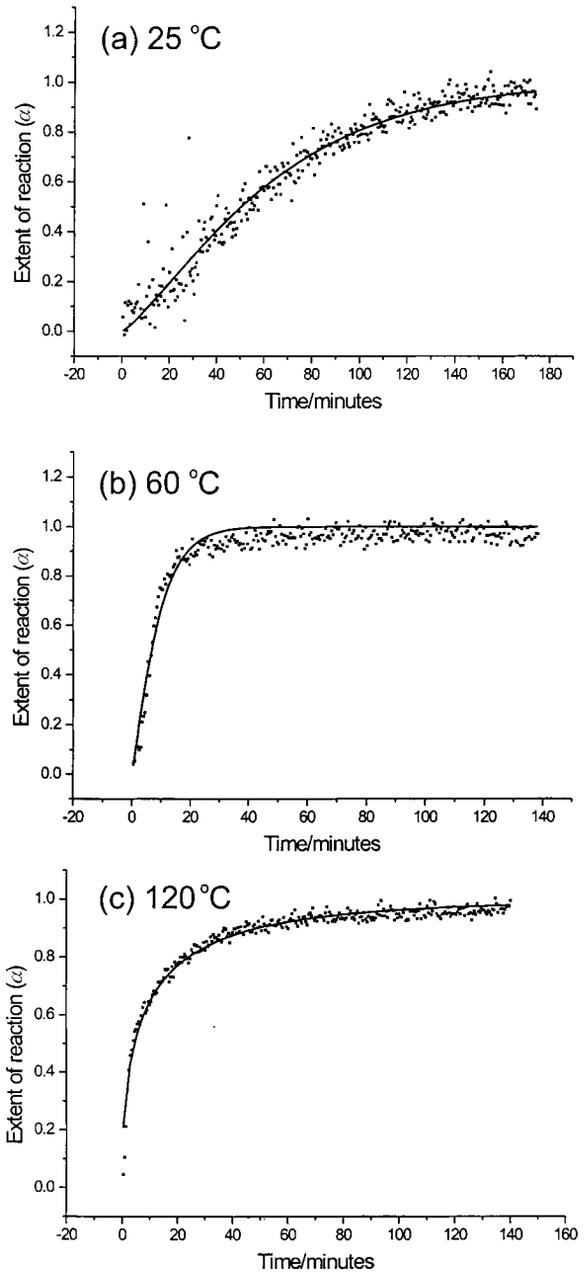

Fig. 7 Normalised peak intensities of the Mg–Al-LDH (003) reflection during reconstruction at three temperatures.

reaction reaches completion at around 3 hours. Although the Bragg reflection of the LDH appears almost immediately for all situations studied, the effect of increasing temperature is apparent, with the reactions at the four highest temperatures ($\geqslant 60\,^{\circ}C$) all taking place in similar times, and those at 40 °C and 25 °C progressively slower. The only previous detailed report of the reconstruction of the Mg–Al–carbonate LDH was performed at room temperature and investigated the effect of repeated calcination and reconstruction.[37] In that study a period of 18 hours was used for the reconstruction; our new results clearly show that the process is much more rapid than previously reported.

The FWHM values of the fitted Gaussians decrease with increasing time at all temperatures studied, consistent with an increasing particle size as the reconstruction proceeds. The peak width decreases from the very beginning of the reconstruction, and the minimum value reached depends on the temperature used. For the energy-dispersive X-ray diffraction experiment Gerward *et al.* showed that the broadening of a Bragg reflection due to small particle size is given by eqn. (1):[38]

$$\beta(E) = \frac{K(1/2hc)}{L\sin\theta} \quad (1)$$

where $\beta(E)$ is the line width of the Bragg reflection in the energy dispersive spectrum (FWHM), K is a constant (0.89), h is Planck's constant, c the velocity of light, L the average crystallite size, and θ the (fixed) angle of the detector. In energy-dispersive diffraction experiments, the resolution of the detector is low and so there is a large experimental contribution to the peak width which must be subtracted to reveal the broadening due to particle size. In our experiment, the instrumental contribution was estimated by measuring a diffraction pattern from a silicon standard, and taking the FWHM of a Bragg reflection appearing at a similar energy to the (003) reflection of the LDH. Although approximations have been made (including the fact that we study one Bragg reflection and can only gain information about particle size in one crystallographic direction), we can obtain estimates of the particle size of the reconstructed Mg–Al-LDH from the *in situ* diffraction data, and compare the values with the LDH before calcination and reconstruction. For a dry sample of pre-made Mg–Al-LDH (*i.e.* before calcination and reconstruction) a FWHM value of 1.05 keV was obtained for the (003) reflection, giving a particle size of ≈ 340 Å, which agrees excellently with the value found using the laboratory diffractometer (see above). Table 1 gives the FWHM values and calculated particle diameters for the final products of each reconstruction reaction studied. It is clear that the particle size of the reconstructed LDH is strongly dependent of temperature and also that at all temperatures applied the reconstructed LDH always has a smaller particle size than the LDH initially prepared by calcination. This effect is consistent with the previous room temperature study which showed a reduction in crystallinity on reconstruction compared to the pre-calcination LDH.[37]

The crystallisation curves obtained by monitoring the growth of the (003) LDH reflection during reconstruction provide a means of quantifying the kinetics of the transformation. We are not able to follow the consumption of poorly-

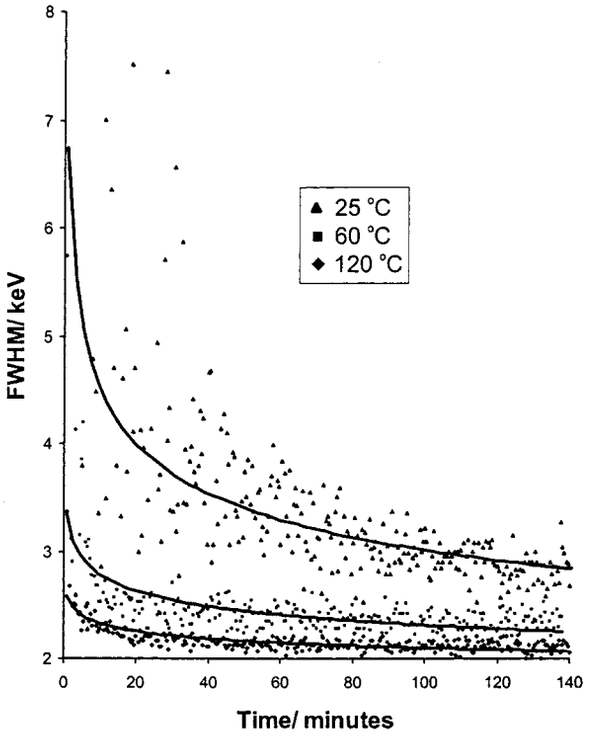

Fig. 8 FWHM of the Mg–Al-LDH (003) reflection during reconstruction at 25 °C, 60 °C and 120 °C.

Table 1 Average particle size after 100 min reconstruction

Material	$FWHM_{measured}$	$FWHM_{corrected}$	Particle size/Å
LDH reference[a]	1.05	0.75	337
Reconstructed 120 °C	2.10	1.80	140
Reconstructed 100 °C	2.15	1.85	137
Reconstructed 80 °C	2.20	1.90	133
Reconstructed 60 °C	2.35	2.05	124
Reconstructed 40 °C	2.55	2.25	112
Reconstructed 25 °C	3.10	2.80	90

[a]Standard LDH before calcination.

ordered LDO, since it exhibits no distinctive diffraction features, but the growth curve of the product contains much information. One simple kinetic model that has been widely applied in solid-state chemistry to model crystallisation and phase transformations is the nucleation–growth model of Avrami and Erofe'ev, eqn. (2),[39–42]

$$\alpha = 1 - \exp\{-(kt)^n\} \quad (2)$$

where α is the extent of reaction scaled from zero at the beginning of reaction and unity at the end, t the time coordinate, k the rate constant and n the Avrami exponent. Although an empirical model, the value of n potentially contains information about the mechanism of the process studied.[43] In choosing a nucleation–growth model to simulate the reconstruction process, we are assuming that the poorly crystalline LDO dissolves in the sodium carbonate solution to give a concentrated solution of reactive species from which nucleation sites for the LDH crystallisation are formed. We believe this is a valid assumption given the huge structural rearrangement taking place in the process, involving the conversion of both Al and Mg in tetrahedral sites in the LDO to both metals in octahedral sites in the LDH as well as incorporation of the hydrated anion. It would be unlikely that this would be a direct solid–solid transformation given the low reaction temperatures used. Least-squares refinements of the Avrami–Erofe'ev expression were performed to the LDH growth curves, and the fits are those shown on Fig. 7 and corresponding parameters are contained in Table 2. Good agreement is observed for the models fitted to the highest and lowest temperature data sets but at intermediate temperatures (*e.g.* 60 °C, Fig. 7b) it proved impossible to obtain a satisfactory fit to the whole extent of data using the simple model of eqn. (1). Examining the kinetic parameters extracted also reveals problems with the simple nucleation–growth model; the value of n appears to vary with temperature, and the rate constant, although smallest at room temperature, follows no obvious pattern over the conditions studied. It may also be observed that the growth curves have distinctly different shapes as the temperatures is changed, indicating changes in reaction mechanism with temperature.

The method of Sharp and Hancock[44] provides an alternative means of extracting kinetic information from the Avrami–Erofe'ev model and for the LDO–LDH conversion allows a greater insight into the possible mechanism. If logarithms are taken twice of the Avrami–Erofe'ev expression, then eqn. (3) is produced.

$$\ln[-\ln(1-\alpha)] = n\ln(t) + n\ln(k) \quad (3)$$

Thus a plot of $\ln[-\ln(1-\alpha)]$ *vs.* $\ln(t)$ will yield a straight line of gradient n and intercept $n\ln(k)$ if the Avrami–Erofe'ev model is valid. Fig. 9 shows such Sharp–Hancock plots for three of the temperatures studied. For reactions performed at room temperature and at 40 °C, a linear plot over the largest part

Table 2 Kinetic parameters determined by least-squares fitting of the Avrami–Erofe'ev expression to the growth curves of Mg–Al–carbonate during reconstruction. n is the Avrami exponent and k the rate constant

Temperature/°C	n	k/min^{-1}
25	1.26	0.015
40	1.43	0.043
60	1.15	0.11
80	0.53	0.11
100	0.55	0.12
120	0.5	0.11

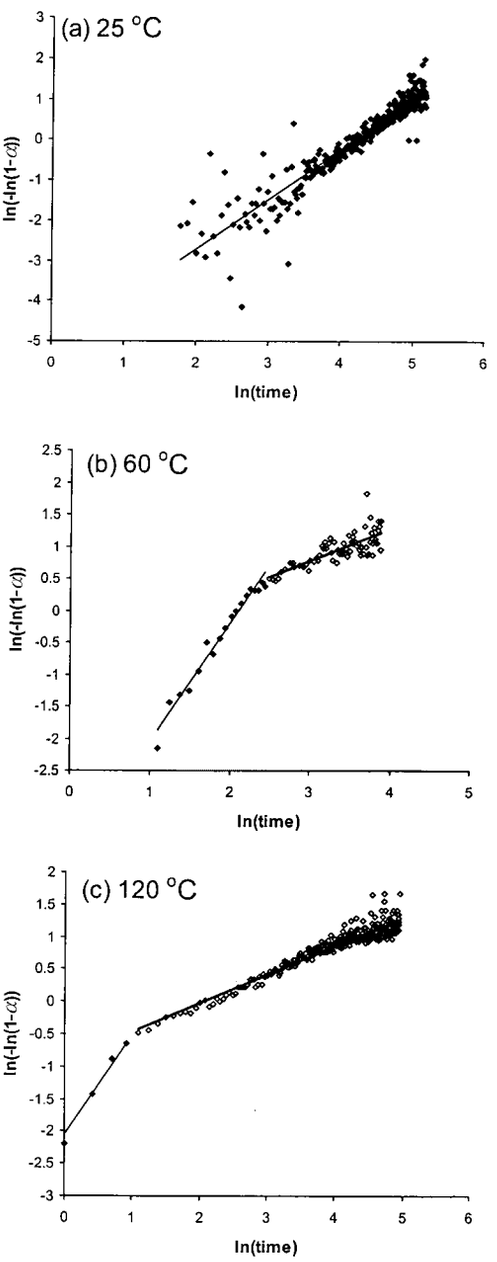

Fig. 9 Sharp–Hancock plots for the crystallisation of Mg–Al-LDH at (a) 25 °C, (b) 60 °C and (c) 120 °C.

Table 3 Kinetic parameters determined by Sharp–Hancock analysis of the reconstruction of Mg–Al–carbonate at various temperatures

Temperature/°C	Stage 1	n_1	k_1/min^{-1}	Stage 2	n_2	k_2/min^{-1}
25	$0.1<\alpha<1.0$	1.22	0.014	—	—	—
40	$0.1<\alpha<1.0$	1.47	0.041	—	—	—
60	$0.1<\alpha<0.75$	1.83	0.120	$0.75<\alpha<1.0$	0.49	0.23
80	$0.1<\alpha<0.6$	2.14	0.180	$0.6<\alpha<1.0$	0.44	0.14
100	$0.1<\alpha<0.5$	1.31	0.220	$0.5<\alpha<1.0$	0.54	0.13
120	$0.1<\alpha<0.45$	1.55	0.270	$0.45<\alpha<1.0$	0.44	0.13

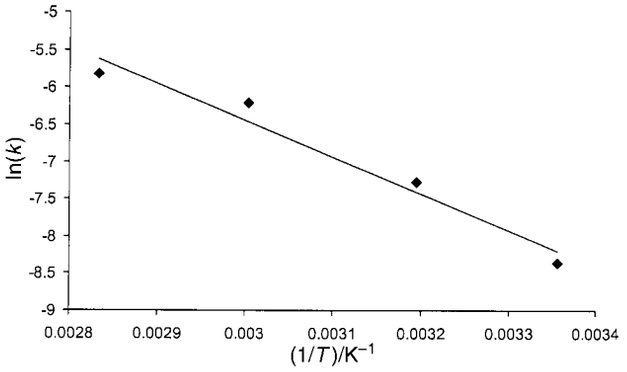

Fig. 10 Arrhenius plot for the nucleation-controlled stage of crystal growth.

of the growth curves is observed and the gradient and intercept were determined by linear regression (Table 3). Data below $\alpha=0.1$ were not included in this analysis as they were subject to the largest experimental errors, due to the difficulty in resolving the Bragg reflection over the background noise at the beginning of the crystallisation. At 60 °C and above two distinct regions of linearity are observed, and these were fitted separately to yield pairs of rate constants and Avrami exponents for each temperature. Inspection of the kinetic parameters in Table 3 suggests that at the higher temperatures studied there are two distinct periods of reaction, each defined by a characteristic value of n, and as the temperature is lowered the second period of reaction shortens from 50% to 25% of the total reaction time until it is no longer detectable at 40 °C, and the reaction takes place in one stage. By considering the scatter on the experimental data points and statistical errors of linear regression we estimate that n can be determined with an accuracy of ±0.5 and k with an error of ±0.02 min^{-1}. The difference in kinetics between the two reaction stages is thus significant.

As was mentioned above the value of the Avrami coefficient contains information about the mechanism of reaction. Although a given value of n does not always unambiguously allow different reaction scenarios to be distinguished, the values of ≈0.5 for the second stage of reaction observed at temperatures of 60 °C and above are consistent with only a diffusion-limited rate of reaction.[43] That is, the rate of crystallisation depends only on the rate of diffusion of the reactive species through the solution to the site of crystallisation, and not on the rate of formation of nucleation sites of crystallisation, the rate of dissolution of the starting materials supplying these species, nor on the rate of crystal growth on the surface of the crystallites. As n becomes larger it is understood that the rate of formation of nucleation sites becomes increasingly important in determining the overall rate of crystallisation. Bearing in mind these concepts we can postulate a model of crystal growth for Mg–Al-LDH by the reconstruction method. At room temperature, the rate of crystallisation is dependent on the rate of formation of nucleation sites for crystal growth to occur ($n\approx1$–2), and the rate of crystal growth at the surface of these nuleation sites and the rate of transport of reactive material to these sites has a minor influence on the overall rate. As the temperature is increased, the rate of nucleation site formation increases and at 60 °C it is ten times that at 25 °C so that part-way through the reaction sufficient nucleation sites have formed that the rate of reaction for the remainder of reaction then only depends on the rate at which reactive material reaches the already-formed sites, *i.e.* the reaction becomes diffusion-limited in the second stage. With a further increase in temperature, the first (nucleation-controlled) stage of reaction becomes progressively shorter as the rate of the nucleation site formation is increased, and at 120 °C the largest part of the reaction becomes diffusion limited. This simple model is consistent with all experimental observations. For example in the diffusion-controlled stage of reaction, when it exists, the rate of crystallisation shows no positive temperature dependence, whereas for the nucleation stage of reaction the rate of crystallisation progressively increases with temperature. Using the rate constants for the first stage of reaction for the four lowest temperatures studied, we can determine the activation energy for the nucleation-controlled crystal growth by an Arrhenius plot (Fig. 10) as 41 kJ mol^{-1}.

Conclusions

The calcination of Mg–Al layered double hydroxides with brucite-type structures have been shown conclusively to produce first a poorly-crystalline mixed Al–Mg oxide (at ≈400 °C) with an MgO-like structure and ultimately a mixture of highly crystalline MgO and $MgAl_2O_4$ (1000 °C). Reaction of the poorly crystalline material with a basic solution containing an anion of interest provides an efficient means of reconstructing the LDH with the anion intercalated. For reconstruction using sodium carbonate solution we have shown the process to be very rapid especially at elevated temperature. *In situ* EDXRD has proved a means of studying the mechanism of reaction, and through the successful modelling of kinetics using the Avrami–Erofe'ev expression we propose that the reaction occurs by dissolution of the highly reactive LDO followed by crystallisation of the LDH from solution.

Acknowledgements

The authors thank Dr. P. Wiseman for his help with the variable temperature XRD measurements. We would like to thank the EPSRC for financial support and provision of synchrotron beamtime at the SRS, Daresbury Laboratory, UK.

References

1 D. W. Bruce and D. O'Hare, *Inorganic Materials*, Wiley, Chichester, 1997.
2 A. Vaccari, *Catal. Today*, 1998, **41**, 53; A. Vaccari, *Appl. Clay Sci.*, 1999, **14**, 161.
3 S. K. Yun and T. J. Pinnavaia, *Chem. Mater.*, 1995, **7**, 348.
4 J. E. Moreyon, A. de Roy, C. Forano and J. P. Besse, *Appl. Clay Sci.*, 1995, **10**, 163.
5 S. M. Auer, R. Wandeler, U. Gobel and A. Baiker, *J. Catal.*, 1997, **169**, 1.
6 F. Basile, L. Basini, M. D. Amore, G. Fornasari, A. Guarinoni,

D. Matteuzzi, G. D. Piero, F. Trifiro and A. Vaccari, *J. Catal.*, 1998, **173**, 247.
7 R. Allmann, *Acta Crystallogr., Sect. B*, 1968, **24**, 972.
8 G. Brown and M. C. Gastuche, *Clay Miner.*, 1967, **7**, 193.
9 S. Miyata, *Clays Clay Miner.*, 1980, **28**, 50.
10 M. Bellotto, B. Rebours, O. Clause, J. Lynch, D. Bazin and E. Elkaim, *J. Phys. Chem.*, 1996, **100**, 8527.
11 J. M. Fernandez, M. A. Ulibarri, F. M. Labojos and V. Rives, *J. Mater. Chem.*, 1998, **8**, 2507.
12 A. M. Fogg, J. S. Dunn, S. G. Shyu, D. R. Cary and D. O'Hare, *Chem. Mater.*, 1998, **10**, 351.
13 W. T. Reichle, *Solid State Ionics*, 1986, **22**, 135.
14 M. Lal and A. T. Howe, *J. Solid State Chem.*, 1986, **39**, 368.
15 T. Lopez, P. Bosch, E. Ramos, R. Gomez, O. Novaro, D. Acosta and F. Figuera, *Langmuir*, 1996, **12**, 189.
16 W. T. Reichle, *Chem. Tech.*, 1986, **16**, 58.
17 F. Cavanni, F. Trifiro and A. Vaccari, *Catal. Today*, 1991, **11**, 173.
18 A. Vaccari, *Chem. Ind.*, 1992, **74**, 174.
19 F. Trifiro and A. Vaccari, in *Comprehensive Supramolecular Chemistry*, ed. J. L. Atwood, J. E. D. Davies, D. D. MacNicol and F. Vogtle, Pergamon, Oxford, UK, 1996, vol. 7, p. 251.
20 E. Kanezaki, *Solid State Ionics*, 1998, **106**, 279; E. Kanezaki, *Inorg. Chem.*, 1998, **37**, 2588.
21 J. Rocha, M. del Arco, V. Rives and M. A. Ulibarri, *J. Mater. Chem.*, 1999, **9**, 2499.
22 I. Rousselot, C. Taviot-Guého and J. P. Besse, *Int. J. Inorg. Mater.*, 1999, **1**, 165.
23 J. S. O. Evans, R. J. Francis, D. O'Hare, S. J. Price, S. M. Clarke, J. Flaherty, J. Gordon, A. Nield and C. C. Tang, *Rev. Sci. Instrum.*, 1995, **66**, 2442.
24 S. M. Clark, A. Nield, T. Rathbone, J. Flaherty, C. C. Tang, J. S. O. Evans, R. J. Francis and D. O'Hare, *Nucl. Instrum. Methods*, 1995, **97**, 98.
25 T. Hibino, Y. Yamashita, K. Kosuge and A. Tsunashima, *Clays Clay Miner.*, 1995, **43**, 427.
26 K. Fuda, N. Kudo, S. Kawai and T. Matsunaga, *Chem. Lett.*, 1993, 777.
27 W. T. Reichle, S. Y. Kang and D. S. Everhardt, *J. Catal.*, 1986, **101**, 352.
28 M. A. Aramendia, Y. Aviles, V. Borau, J. M. Luque, J. M. Marinas, J. R. Ruiz and F. Urbano, *J. Mater. Chem.*, 1999, **9**, 1603.
29 A. S. Bookin and A. Drits, *Clays Clay Miner.*, 1993, **41**, 558.
30 M. A. Drezdzon, *Inorg. Chem.*, 1988, **27**, 4628.
31 V. Rives, *Inorg. Chem.*, 1999, **38**, 406.
32 P. Malet, O. Prieto, V. Rives, R. Trujilano, C. Barriga, J. M. Ferandez and M. A. Ulibarri, *Synchrotron Radiation Department Scientific Reports 1997–1998*, CLRC Daresbury Laboratory, UK, p. 364, 1999.
33 J. T. Kloprogge and R. L. Frost, *J. Solid State Chem.*, 1999, **146**, 506.
34 M. A. Aramendia, V. Borau, C. Jimenez, J. M. Marinas, F. J. Romero, J. Navio and J. Barrios, *J. Catal.*, 1995, **157**, 97.
35 J. Munn, P. Barnes, D. Hausermann, S. A. Axon and J. Klinowski, *Phase Transitions*, 1992, **39**, 129.
36 S. M. Clark, *J. Appl. Crystallogr.*, 1995, **28**, 646.
37 T. Hibino and A. Tsunashima, *Chem. Mater.*, 1998, **10**, 4055.
38 L. Gerward, S. Mørup and H. Topsøe, *J. Appl. Phys.*, 1976, **47**, 822.
39 M. Avrami, *J. Chem. Phys.*, 1939, **7**, 1103.
40 M. Avrami, *J. Chem. Phys.*, 1940, **8**, 212.
41 M. Avrami, *J. Chem. Phys.*, 1941, **9**, 177.
42 B. V. Erofe'ev, *C. R.. Dokl. Acad. Sci. URSS*, 1946, **52**, 511.
43 S. F. Hulbert, *J. Br. Ceram. Soc.*, 1969, **6**, 11.
44 J. D. Sharp and J. H. Hancock, *J. Am. Chem. Soc.*, 1972, **55**, 74.